Quantum Teleportation State Explorer

Arda Çelik[1], Ege Erçiftçi[1], Mustafa Öztürk[1], Yusuf Kayra Gül[1] and Muhammad Shahryar Khan[1]

[1]*Department of Physics, Bilkent University*

May 20, 2026

1. BACKGROUND AND CONTINUOUS-VARIABLE TELEPORTATION

Quantum teleportation is a protocol for transferring an unknown quantum state from a sender, Alice, to a distant receiver, Bob, without physically transporting the physical system itself. The essential ingredients are a shared entangled resource, a measurement performed by Alice, classical communication of the measurement result, and a correction operation applied by Bob. The role of entanglement is to provide nonclassical correlations between Alice and Bob, while the role of the classical channel is to tell Bob which correction operation must be applied. Since this correction depends on Alice's classical message, teleportation does not allow faster-than-light communication.

The original teleportation protocol was proposed by Bennett et al. for discrete-variable systems [3]. In the simplest version, the input state is a qubit,

$$|\psi\rangle = \alpha|0\rangle + \beta|1\rangle, \qquad |\alpha|^2 + |\beta|^2 = 1. \tag{1}$$

Alice and Bob share an entangled Bell pair. Alice performs a Bell-state measurement on the unknown qubit and her half of the Bell pair. The measurement outcome is sent to Bob through a classical channel. Bob then applies the corresponding unitary correction, after which his system is left in the original state. This discrete-variable protocol is conceptually simple because the Hilbert space is finite-dimensional.

Continuous-variable teleportation extends the same idea to systems described by observables with continuous spectra. In quantum optics, the natural variables are the quadratures of a bosonic field mode,

$$\hat{x} = \frac{\hat{a} + \hat{a}^\dagger}{\sqrt{2}}, \qquad \hat{p} = \frac{\hat{a} - \hat{a}^\dagger}{i\sqrt{2}}, \tag{2}$$

where $\hat{a}$ and $\hat{a}^\dagger$ are annihilation and creation operators satisfying

$$[\hat{a}, \hat{a}^\dagger] = 1. \tag{3}$$

With this convention,

$$[\hat{x}, \hat{p}] = i, \qquad \Delta x_{\mathrm{vac}}^2 = \Delta p_{\mathrm{vac}}^2 = \frac{1}{2}. \tag{4}$$

Unlike a qubit, an optical mode lives in an infinite-dimensional Hilbert space. This makes the system richer but also numerically more demanding.

The standard continuous-variable teleportation protocol is the Braunstein–Kimble protocol [5]. Instead of sharing a Bell pair of qubits, Alice and Bob share an EPR-like two-mode squeezed state. In the ideal EPR limit, the two shared modes A and B satisfy perfect quadrature correlations,

$$\hat{x}_A - \hat{x}_B = 0, \qquad \hat{p}_A + \hat{p}_B = 0. \tag{5}$$

These exact correlations are unphysical because they require infinite energy. Experimentally, they are approximated by a two-mode squeezed vacuum state,

$$|\mathrm{TMSV}\rangle_{AB} = \sqrt{1-\lambda^2}\sum_{n=0}^{\infty} \lambda^n |n\rangle_A |n\rangle_B, \qquad \lambda = \tanh r, \tag{6}$$

where r is the squeezing parameter. Larger r corresponds to stronger EPR correlations and therefore better teleportation quality.

In the Braunstein–Kimble protocol, Alice mixes the unknown input mode with her half of the entangled resource using a balanced beam splitter. She then measures two commuting quadrature combinations,

$$\hat{x}_- = \frac{\hat{x}_1 - \hat{x}_2}{\sqrt{2}}, \qquad \hat{p}_+ = \frac{\hat{p}_1 + \hat{p}_2}{\sqrt{2}}. \tag{7}$$

The measurement outcomes are classical real numbers, so Alice can send them to Bob. Bob then applies a phase-space displacement to his mode. In the ideal unit-gain EPR limit, Bob reconstructs the input quadratures,

$$\hat{x}_{\text{out}} = \hat{x}_{\text{in}}, \qquad \hat{p}_{\text{out}} = \hat{p}_{\text{in}}, \tag{8}$$

so that

$$\rho_{\text{out}} = \rho_{\text{in}}. \tag{9}$$

The first unconditional experimental demonstration of continuous-variable teleportation of optical coherent states was reported by Furusawa et al. [6]. In realistic implementations, however, the ideal EPR correlations are degraded by finite squeezing, detector inefficiency, optical loss, thermal noise, phase diffusion, imperfect feed-forward, and mode mismatch. Therefore, realistic continuous-variable teleportation must be treated as a noisy quantum channel rather than a perfect identity operation. This non-ideal channel picture is the starting point of our numerical work.

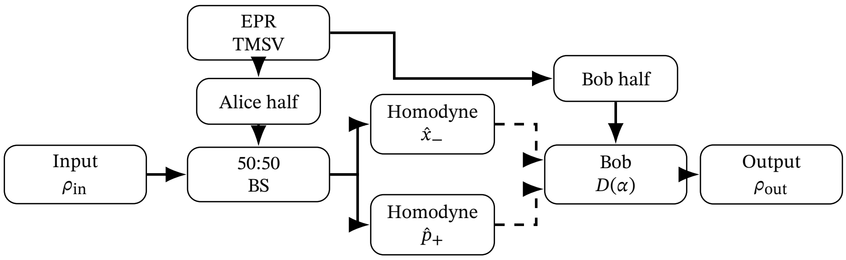

Figure 1. Schematic of the Braunstein–Kimble continuous-variable teleportation protocol. Alice mixes the unknown input state with her half of the EPR resource, performs homodyne measurements, sends the classical outcomes to Bob, and Bob applies a displacement correction.

2. PHASE-SPACE CHANNEL MODEL

2.1. Truncated Fock-Space Representation

A single optical mode can be represented in the Fock basis as

$$|\psi\rangle = \sum_{n=0}^{\infty} c_n |n\rangle, \qquad \sum_{n=0}^{\infty} |c_n|^2 = 1. \tag{10}$$

In numerical work, this infinite-dimensional space must be truncated:

$$|\psi\rangle \approx \sum_{n=0}^{N_{\text{cut}}-1} c_n |n\rangle. \tag{11}$$

The cutoff N_{cut} is not only a technical detail; it directly affects the reliability of the simulation. If a state has significant population near $n = N_{\text{cut}} - 1$, then the truncation is too small. This is especially important for states with large displacement, large mean photon number, or fine phase-space structure. It is also important when the teleportation channel contains strong noise, because random displacements can move the state into regions requiring higher photon-number components.

The corresponding density matrix is

$$\rho = |\psi\rangle\langle\psi|. \tag{12}$$

For pure input states, the code usually stores both the ket $|\psi\rangle$ and the density matrix ρ. The ket is useful for evaluating pure-state fidelity, while the density matrix is the object acted on by the noisy channel. This is the logic behind the QuTiP-based notebook implementation, where states such as coherent, squeezed, Fock, cat, compass, and approximate GKP-like states are constructed in a finite Fock basis [11, 12].

In practice, one should choose N_{cut} according to the energy and phase-space extent of the state. For example, a coherent state with $|\alpha|^2 \approx 1$ can be represented accurately with a modest cutoff, while approximate GKP-like states and large compass states may need much larger cutoffs. In our app, the cutoff is treated as a user-controlled numerical parameter, and selected results are compared between $N_{\text{cut}} = 10$ and $N_{\text{cut}} = 30$ to check whether the optimized state is stable.

2.2. Wigner Representation and Phase-Space Intuition

Our numerical analysis is mainly formulated in phase space using the Wigner function $W(x, p)$. The Wigner function is a real quasi-probability distribution over the two quadratures x and p [1, 2]. It is normalized as

$$\int_{\mathbb{R}^2} W(x, p)\, dx\, dp = 1. \tag{13}$$

For the vacuum state, using our quadrature convention,

$$W_0(x, p) = \frac{1}{\pi} \exp(-x^2 - p^2). \tag{14}$$

The Wigner representation is useful for two reasons. First, it gives a direct visual interpretation of the input and output states. A coherent state appears as a smooth Gaussian blob, a squeezed state appears as an elliptical Gaussian, a Fock state shows a negative central region, a cat state shows two coherent peaks and interference fringes, and GKP-like states show grid-like structure. Second, the non-ideal continuous-variable teleportation channel acts naturally as a phase-space blurring operation. Therefore, the Wigner function makes it visually clear why different states respond differently to the same noisy channel.

In the app, Wigner functions are evaluated on a finite grid. This introduces two numerical parameters: the grid range and the grid resolution. The grid range must be large enough that the Wigner function does not get clipped, while the resolution must be high enough to capture interference fringes and negative regions. These requirements are mild for coherent states but much stricter for cat, compass, and approximate GKP-like states.

2.3. Effective Gaussian Channel

We write the quadrature vector as

$$\hat{\xi} = \begin{pmatrix} \hat{x} \\ \hat{p} \end{pmatrix}. \tag{15}$$

A noisy single-mode teleportation channel can be modeled as

$$\hat{\xi}_{\text{out}} = G\hat{\xi}_{\text{in}} + \hat{n}_{\text{eff}}, \tag{16}$$

where G is a gain matrix and $\hat{n}_{\text{eff}}$ is an effective noise vector. In the simplest case,

$$G = gI_2, \tag{17}$$

where g is the scalar feed-forward gain. The effective noise is characterized by its covariance matrix,

$$Y = \langle \hat{n}_{\text{eff}} \hat{n}_{\text{eff}}^T \rangle = \begin{pmatrix} \nu_x & \nu_{xp} \\ \nu_{xp} & \nu_p \end{pmatrix}. \tag{18}$$

The ideal teleportation limit is recovered for

$$G = I_2, \qquad Y = 0. \tag{19}$$

In Wigner space, the gain/noise part of the channel acts as a Gaussian convolution,

$$W_{\text{out}}(\xi) = \int_{\mathbb{R}^2} G_Y(\xi - g\xi' - d) W_{\text{in}}(\xi')\, d^2\xi', \tag{20}$$

where $\xi = (x, p)^T$, $d = (d_x, d_p)^T$ is an optional displacement drift, and

$$G_Y(\xi) = \frac{1}{2\pi\sqrt{\det Y}} \exp\left[-\frac{1}{2}\xi^T Y^{-1} \xi\right]. \tag{21}$$

This form shows that the output is a blurred version of the input. In the app, this Wigner-space expression is the main channel model.

In the notebook, an equivalent density-matrix picture is used for simple isotropic displacement noise,

$$\rho_{\text{out}} = \int d^2\beta\, P(\beta) D(\beta) \rho_{\text{in}} D^\dagger(\beta), \tag{22}$$

where $D(\beta)$ is the displacement operator. Numerically, the integral is approximated by Gauss–Hermite quadrature. The code therefore loops over quadrature points and weights, applies displacement operators, and averages the displaced density matrices. This method gives a transparent way to understand noisy teleportation: Bob receives an average over many randomly shifted copies of Alice's input state.

2.4. Finite Squeezing and Detector Inefficiency

Finite squeezing is the dominant imperfection in the Braunstein–Kimble protocol. In the ideal EPR resource, the residual noises δx and δp vanish. For finite squeezing they remain nonzero. In the symmetric unit-gain model, the corresponding effective noise contribution scales as

$$\nu_{\text{sq}}(r) = e^{-2r}. \tag{23}$$

Therefore increasing r improves the teleportation channel.

Detector inefficiency also adds noise. If η is the homodyne detection efficiency, a simple effective model gives

$$\nu_{\text{det}}(\eta) = \frac{1-\eta}{2\eta}. \tag{24}$$

Combining finite squeezing and detector inefficiency gives

$$\nu_{\text{eff}} = e^{-2r} + \frac{1-\eta}{2\eta}. \tag{25}$$

The corresponding isotropic covariance matrix is

$$Y_{\text{eff}} = \nu_{\text{eff}} \begin{pmatrix} 1 & 0 \\ 0 & 1 \end{pmatrix}. \tag{26}$$

Equation (25) explains the basic trends of the first numerical sweeps: fidelity improves as r increases and as η approaches unity. However, the expression also diverges as $\eta \to 0$, so very low detector efficiencies are numerically difficult in a finite-dimensional simulation.

2.5. Asymmetric, Rotated, and Correlated Noise

A scalar noise strength is not enough to describe all realistic non-ideal EPR resources. The app therefore allows the covariance matrix Y to have different geometries. In the anisotropic case,

$$Y_{\text{aniso}} = \begin{pmatrix} \nu_x & 0 \\ 0 & \nu_p \end{pmatrix}, \qquad \nu_x \neq \nu_p. \tag{27}$$

This models unequal noise in the two quadratures. It is especially important for squeezed states and oriented cat states, because their robustness depends on which quadrature is noisier.

A more general model includes correlated EPR noise,

$$Y_{\text{corr}} = \begin{pmatrix} \nu_x & \rho\sqrt{\nu_x \nu_p} \\ \rho\sqrt{\nu_x \nu_p} & \nu_p \end{pmatrix}, \tag{28}$$

where ρ is a correlation coefficient. The app also includes rotated anisotropic noise,

$$Y(\theta) = R(\theta) Y_0 R^T(\theta). \tag{29}$$

The rotation matrix is

$$R(\theta) = \begin{pmatrix} \cos\theta & -\sin\theta \\ \sin\theta & \cos\theta \end{pmatrix}. \tag{30}$$

These models make the project more than a simple fidelity-versus-squeezing study. They allow us to ask whether a state's teleportation performance depends on the direction and correlation structure of the noise in phase space.

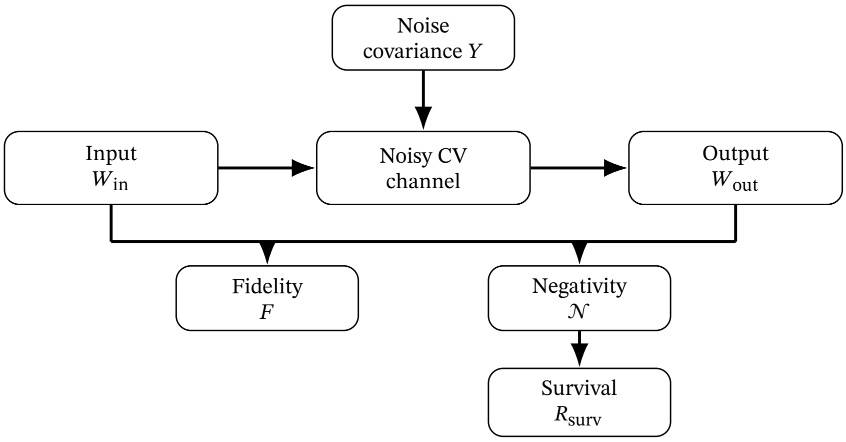

Figure 2. Summary of the phase-space channel model and diagnostics. The noisy continuous-variable teleportation channel maps the input Wigner function to a blurred output Wigner function. Fidelity measures input-output overlap, while Wigner negativity and the survival ratio quantify how much nonclassical phase-space structure remains.

3. INPUT STATES AND DIAGNOSTICS

3.1. Reference States

The first part of the numerical study compares physically motivated reference states. This gives a baseline for interpreting the optimized states produced by the app.

The coherent state,

$$|\psi_{\text{coh}}\rangle = |\alpha\rangle, \tag{31}$$

is the standard benchmark. It has a smooth Gaussian Wigner function and is the closest quantum analogue of a classical optical field. For coherent-state teleportation, the classical benchmark $F_{\text{cl}} = 1/2$ is often used.

The squeezed vacuum state is

$$|\psi_{\text{sq}}\rangle = S(s)|0\rangle, \tag{32}$$

where $S(s)$ is the single-mode squeezing operator. It is still Gaussian, but it is nonclassical because one quadrature variance is reduced below the vacuum level. Its teleportation performance depends strongly on whether the added noise is aligned with the squeezed quadrature.

The single-photon Fock state is

$$|\psi_{\text{Fock}}\rangle = |1\rangle. \tag{33}$$

This state is non-Gaussian and has Wigner negativity. It is a useful simple test of whether the channel preserves nonclassicality.

We also use even and odd cat states [4, 10],

$$|\psi_{\text{even}}\rangle = \mathcal{N}_+ \left(|\alpha\rangle + |-\alpha\rangle\right), \qquad |\psi_{\text{odd}}\rangle = \mathcal{N}_- \left(|\alpha\rangle - |-\alpha\rangle\right). \tag{34}$$

Cat states are superpositions of two coherent states separated in phase space. Their Wigner functions contain interference fringes between the two coherent peaks, and those fringes are highly sensitive to Gaussian displacement noise.

The compass state is a four-component coherent-state superposition,

$$|\psi_{\text{comp}}\rangle = \mathcal{N}_{\text{comp}} \left(|\alpha\rangle + |-\alpha\rangle + |i\alpha\rangle + |-i\alpha\rangle\right). \tag{35}$$

It has interference structure in both quadrature directions, so it is expected to be more fragile than a two-component cat state.

Finally, we include an approximate GKP-like state. Ideal GKP states are grid states in phase space and require infinite energy [7]. Our simulations use finite-energy approximations. Because approximate GKP states have fine phase-space structure, they are especially sensitive to displacement noise and Wigner-grid resolution.

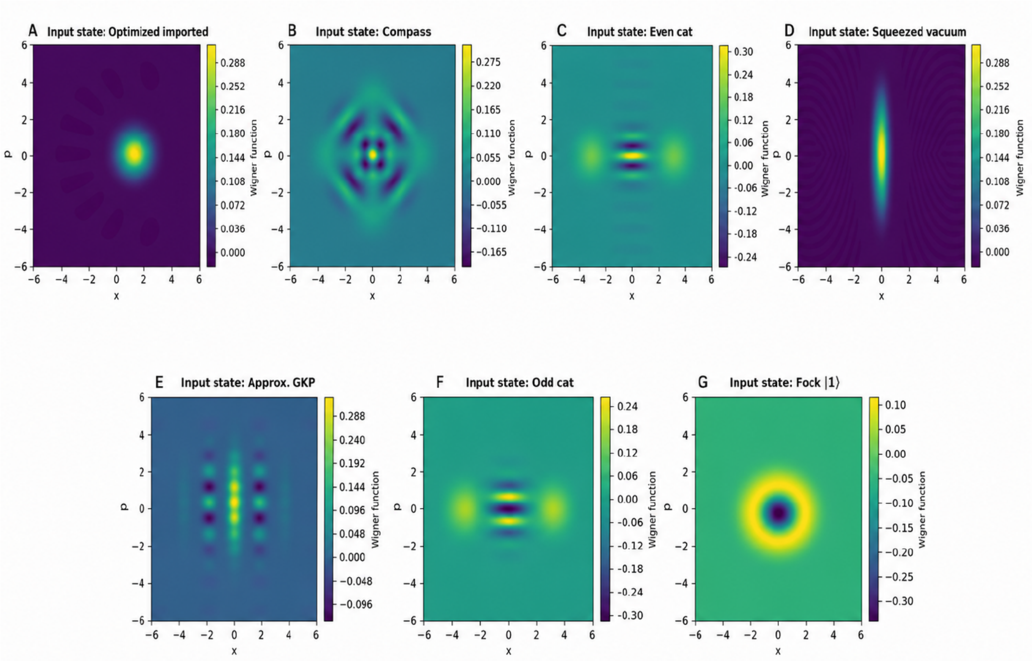

Figure 3. Input Wigner functions of the reference states used in the numerical comparison. The coherent and squeezed states have smooth Gaussian structure, while Fock, cat, compass, and approximate GKP-like states contain Wigner negativity, interference fringes, or grid-like phase-space structure.

3.2. Fidelity

For a pure input state $|\psi\rangle$, the teleportation fidelity is

$$F(\psi) = \langle\psi|\rho_{\mathrm{out}}|\psi\rangle. \tag{36}$$

This is the main performance metric used throughout the report. If $F = 1$, the output state is identical to the input. Smaller values indicate that the channel has distorted the state.

In Wigner space, the same fidelity can be written as an overlap integral [8],

$$F(\psi) = 2\pi \int_{\mathbb{R}^2} W_{\mathrm{in}}(x,p)W_{\mathrm{out}}(x,p)\,dx\,dp. \tag{37}$$

This formula is especially useful in the app because both the input and output states are represented on a Wigner grid. It also gives a simple geometric interpretation: high fidelity means that the input and output Wigner functions strongly overlap.

3.3. Wigner Negativity and Survival Ratio

Fidelity alone does not always tell us whether nonclassicality survives. A noisy output can still have moderate overlap with the input while losing most of its negative Wigner volume. For this reason we also use Wigner negativity [9],

$$\mathcal{N}(W) = \frac{1}{2}\int_{\mathbb{R}^2} (|W(x,p)| - W(x,p))\,dx\,dp. \tag{38}$$

If $W(x,p) \geq 0$ everywhere, then $\mathcal{N}(W) = 0$. Coherent and Gaussian squeezed states do not have Wigner negativity. Fock states, cat states, compass states, and approximate GKP-like states can have $\mathcal{N}(W) > 0$.

For states with nonzero input negativity, we define the negativity survival ratio

$$R_{\mathrm{surv}} = \frac{\mathcal{N}(W_{\mathrm{out}})}{\mathcal{N}(W_{\mathrm{in}})}. \tag{39}$$

This ratio measures how much of the input nonclassicality remains after teleportation. It is one of the main diagnostics used in the nonclassicality-survival part of the project.

4. STANDARD NUMERICAL CASE STUDIES

4.1. Input-State Wigner Functions

The first numerical step is to visualize the input Wigner functions. This step is not merely decorative; it explains why different states respond differently to the same channel. Since the channel acts as a phase-space blurring operation, states with smooth Wigner functions are expected to be more robust than states with fine interference patterns.

The coherent state appears as a single smooth Gaussian peak. The squeezed state is still Gaussian but elongated in one direction and compressed in the other. The Fock state $|1\rangle$ has a negative central region. The even and odd cat states have two separated coherent peaks with interference fringes between them. The compass state contains interference structure in both quadrature directions. The approximate GKP-like state contains a grid-like pattern. These observations give the qualitative expectation for the fidelity and negativity-survival plots.

4.2. Fidelity Versus Squeezing

We first study the dependence of fidelity on the squeezing parameter r. For each input state, we compute

$$F(r) = \langle\psi|\mathcal{E}_r(|\psi\rangle\langle\psi|)|\psi\rangle. \tag{40}$$

Since the finite-squeezing noise scales as e^{-2r}, increasing r should reduce the channel noise.

The numerical results in Fig. 4 show the expected trend: fidelity increases as r increases. The coherent state has the highest fidelity over much of the parameter range because it is a smooth Gaussian state. The squeezed state also performs well, but its fidelity depends more strongly on quadrature noise. Non-Gaussian states such as Fock, cat, compass, and approximate GKP-like states require larger squeezing to reach comparable fidelities.

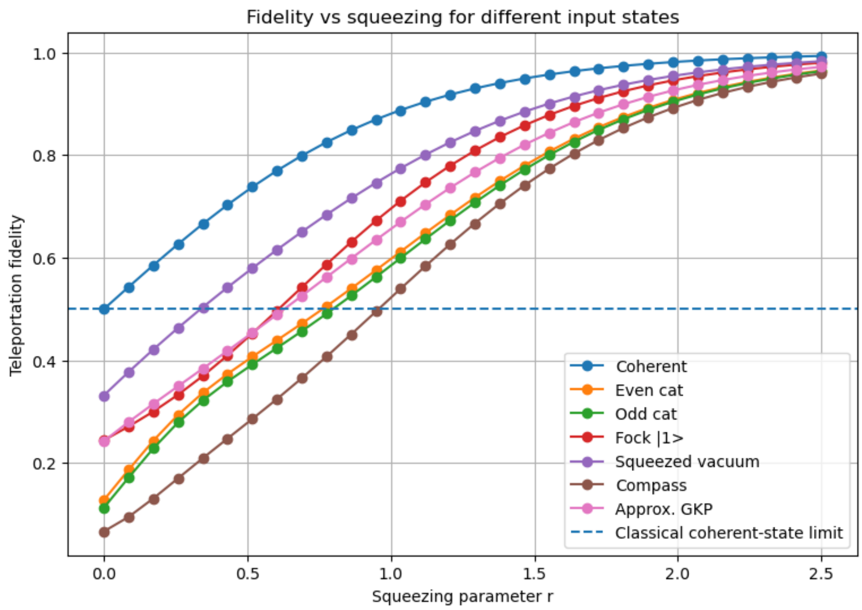

Figure 4. Teleportation fidelity versus squeezing parameter r for different input states. Increasing r reduces finite-squeezing noise, so all fidelities increase toward unity. Coherent states are the most robust, while non-Gaussian states require stronger squeezing to reach comparable fidelity.

4.3. Fidelity Versus Detector Efficiency

The detector-efficiency sweep studies

$$F(\eta) = \langle\psi|\mathcal{E}_\eta(|\psi\rangle\langle\psi|)|\psi\rangle. \tag{41}$$

Because the effective detector noise is

$$\nu_{\mathrm{det}}(\eta) = \frac{1-\eta}{2\eta}, \tag{42}$$

the physical expectation is that fidelity should improve as η increases.

The moderate-to-high η region follows the expected trend in Fig. 5. At very low η, however, the effective noise becomes very large. In this region, finite Fock cutoffs and finite Wigner grids may produce artificial oscillations or non-monotonic behavior. Therefore, low-η features should not be overinterpreted unless convergence is checked by increasing N_{cut}, increasing the Wigner-grid range, and increasing the grid resolution.

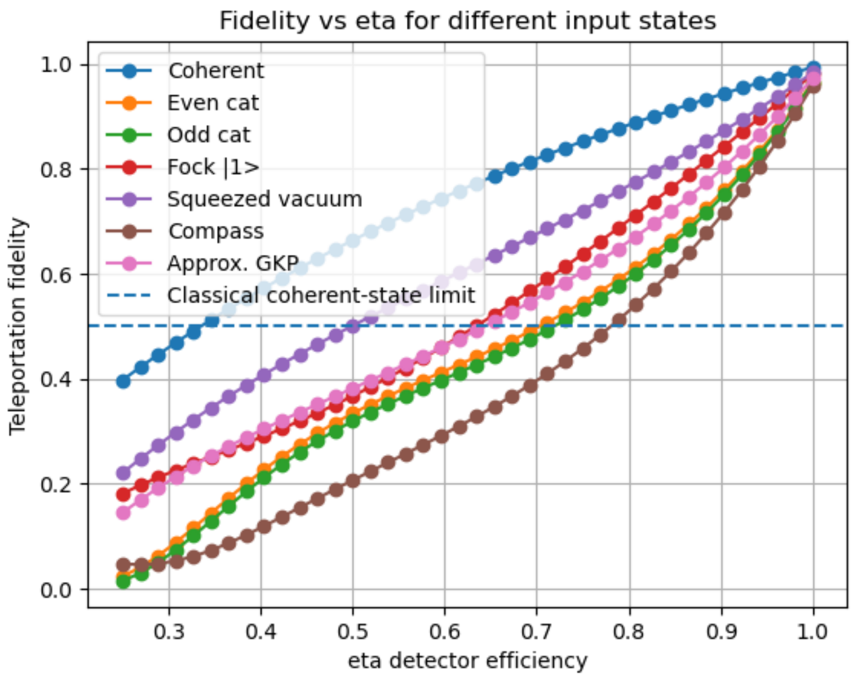

Figure 5. Teleportation fidelity versus detector efficiency η. Fidelity increases as detector efficiency improves. The plot focuses on the moderate-to-high efficiency regime, where the effective detector noise is numerically better behaved than in the very low-η limit.

4.4. EPR Noise Geometry

The EPR-noise geometry study is one of the most original parts of the project. Instead of using only isotropic noise, we vary the direction and correlation structure of the noise. The three main cases are asymmetric quadrature noise, rotated asymmetric noise, and correlated non-ideal EPR noise.

In the asymmetric case, the two quadratures have different effective noise variances, $\nu_x \neq \nu_p$. This directly tests whether a state is more sensitive to noise in the x- or p-direction. As shown in Fig. 6, changing the noise asymmetry can strongly change the relative ordering of the input states. This is expected because squeezed states, cat states, compass states, and approximate GKP-like states have directional phase-space structure.

In the correlated-noise case, the off-diagonal covariance term ν_{xp} is varied through the correlation coefficient ρ. Figure 7 shows that the fidelity can vary with ρ, although the strength of this dependence is state-dependent. Coherent states remain relatively stable, while non-Gaussian states show stronger sensitivity.

In the rotated-noise case, the anisotropic noise ellipse is rotated relative to the input state's Wigner function. Figure 8 shows that the rotation angle can significantly affect squeezed and non-Gaussian states. This confirms that teleportation quality depends not only on the total amount of noise, but also on its phase-space orientation.

4.5. Nonclassicality Survival

We then compute Wigner-negativity survival:

$$R_{\text{surv}} = \frac{\mathcal{N}(W_{\text{out}})}{\mathcal{N}(W_{\text{in}})}. \tag{43}$$

This quantity is meaningful only for states with nonzero input negativity.

Figure 9 shows that Wigner negativity is more fragile than ordinary fidelity. For some states, the survival ratio remains low even when the corresponding fidelity is moderate. This means that the output state can still overlap with the input while losing much of its genuinely nonclassical phase-space structure.

The Fock state shows strong negativity survival at larger squeezing, while cat states recover more slowly. Compass and approximate GKP-like states also show substantial sensitivity because their Wigner negativity is distributed in finer phase-space structures. This result supports one of the main messages of the project: preserving nonclassicality is a stricter requirement than preserving ordinary state overlap.

5. QUANTUM TELEPORTATION STATE EXPLORER AND OPTIMIZATION

5.1. Motivation and Role of the App

A central contribution of this project is the *Quantum Teleportation State Explorer*. The app was developed because ordinary parameter sweeps are not enough to answer the most interesting question: for a given noisy teleportation channel, which input state performs best under fixed physical constraints?

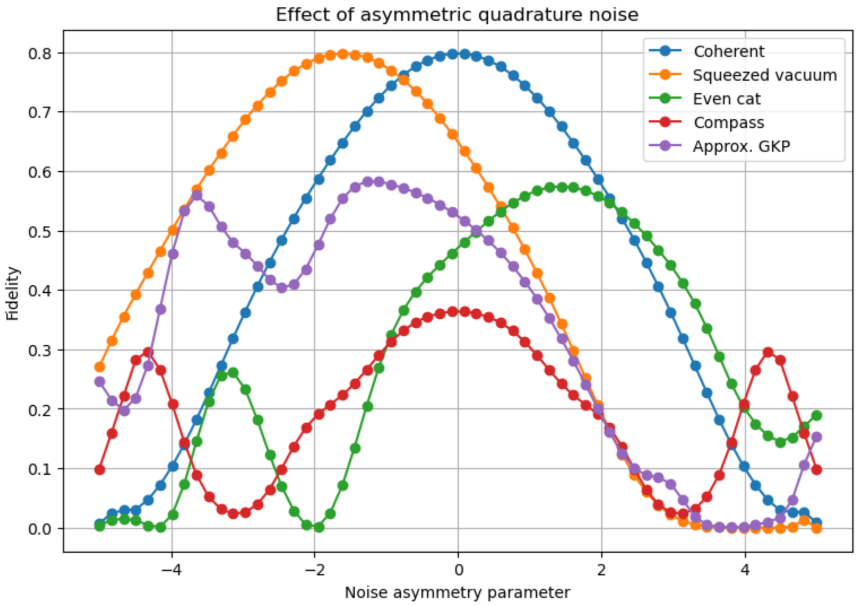

Figure 6. Effect of asymmetric quadrature noise on teleportation fidelity. The noise asymmetry changes the relative performance of the input states because each state has a different phase-space orientation and structure.

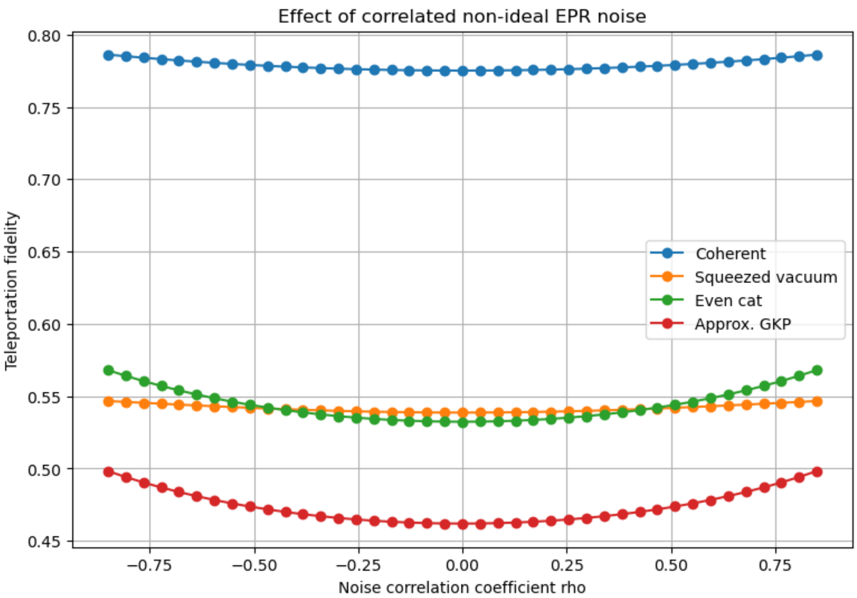

Figure 7. Effect of correlated non-ideal EPR noise on teleportation fidelity. The correlation coefficient ρ changes the shape of the Gaussian noise kernel in phase space. Different input states respond differently to this correlation structure.

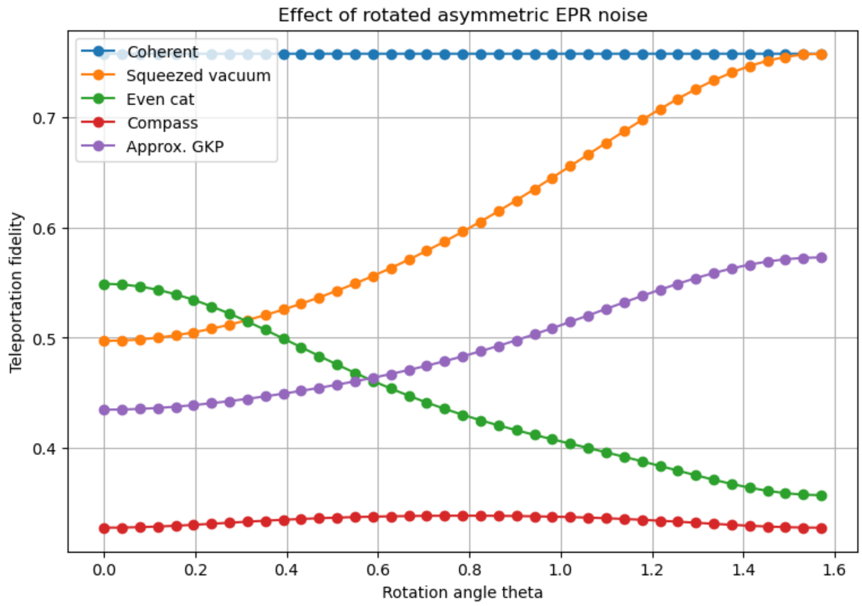

Figure 8. Effect of rotated asymmetric EPR noise on teleportation fidelity. The rotation angle changes the orientation of the noise ellipse relative to the input state's Wigner function. This particularly affects phase-sensitive states such as squeezed, cat, compass, and approximate GKP-like states.

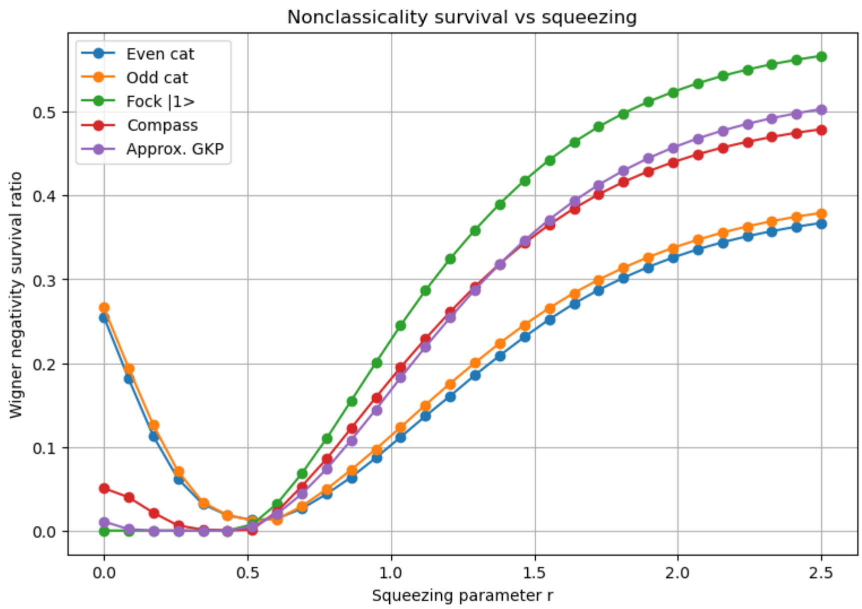

Figure 9. Wigner-negativity survival ratio versus squeezing parameter r. Increasing squeezing generally improves survival of nonclassicality, but the recovery rate depends strongly on the input state. This shows that fidelity and nonclassicality preservation are related but not equivalent diagnostics.

The app has two roles. First, it is a forward simulator. Given an input state and a noisy channel, it computes the output Wigner function, fidelity, Wigner negativity, and survival ratio. Second, it is an inverse-design tool. Instead of choosing the input state by hand, it searches over a family of truncated Fock-basis states and tries to find a state adapted to the selected channel.

This is the main difference between the app and a standard notebook simulation. The notebook is useful for transparent calculations and simple sweeps. The app makes it possible to optimize states, compare them with references, save or import channels, and study how the optimal state changes when the noise model or objective function is changed.

The app is therefore not only a visualization interface. It is the main numerical contribution of the project. It combines state preparation, channel simulation, Wigner diagnostics, constrained optimization, and reference-state benchmarking in a single workflow. This makes the project closer to an inverse-design study than a purely textbook simulation of continuous-variable teleportation.

5.2. State Parameterization

The optimized state is written as

$$|\psi_{\mathrm{opt}}\rangle = \sum_{n=0}^{N_{\mathrm{cut}}-1} c_n |n\rangle. \tag{44}$$

The complex coefficients c_n are the optimization variables. Equivalently, each coefficient can be written as

$$c_n = x_n + i y_n, \tag{45}$$

so the optimizer works over real variables x_n and y_n. The normalization constraint is

$$\sum_{n=0}^{N_{\mathrm{cut}}-1} |c_n|^2 = 1. \tag{46}$$

The fixed-energy constraint is

$$\langle \hat{n} \rangle = \sum_{n=0}^{N_{\mathrm{cut}}-1} n |c_n|^2 = N_{\mathrm{target}}. \tag{47}$$

This constraint is important because otherwise the optimizer could improve the objective simply by changing the physical energy of the state. Fixing $\langle \hat{n} \rangle$ makes comparisons with reference states more meaningful.

The optimization variables therefore define a general pure state inside a finite-dimensional Hilbert space. Unlike coherent or cat states, the optimized state is not assumed to have a predetermined analytic form. This is why the resulting Wigner function must be inspected: it tells us what kind of state the optimizer has actually found.

5.3. Objective Functions

The default objective is fidelity maximization:

$$\max_{\psi} F(\psi) = \max_{\psi} \langle \psi | \mathcal{E}(|\psi\rangle\langle\psi|) |\psi\rangle. \tag{48}$$

This objective asks for the state that best survives the selected noisy teleportation channel in the sense of input-output overlap.

The app also allows objectives involving Wigner-negativity survival. A schematic form is

$$S(\psi) = w_F F(\psi) + w_R R_{\mathrm{surv}}(\psi), \tag{49}$$

where w_F and w_R are user-chosen weights. This objective is qualitatively different from pure-fidelity optimization. A pure-fidelity objective often favors smooth Gaussian-like states because they are robust under Gaussian blurring. A negativity-survival objective encourages states with nonclassical Wigner structure that remains after teleportation.

5.4. Optional Constraints and Channel Configuration

In addition to normalization and fixed energy, the app includes optional constraints such as even or odd parity, bounds on displacement, restrictions on Fock support, limits on high-Fock tail population, constraints on photon-number statistics, quadrature-variance constraints, Wigner-negativity constraints, and overlap constraints with reference states. These constraints prevent the optimizer from finding mathematically high-scoring but physically uninteresting states.

The app also allows the user to configure the noisy teleportation channel. The most important parameters are squeezing r, detector efficiency η, feed-forward gain g, anisotropic noise parameters ν_x, ν_p, rotation angle θ, correlation coefficient ρ, thermal noise, transmissivity or loss-like noise, phase diffusion strength, and deterministic displacement drift. This flexibility is important because realistic teleportation quality cannot be described by only one scalar parameter.

5.5. Outputs and Validation Quantities

After a simulation or optimization, the app reports input and output Wigner functions, teleportation fidelity, input and output Wigner negativity, negativity survival ratio, Wigner-shape overlap, mean photon number, parity expectation, high-Fock tail population, and constraint satisfaction. These diagnostics are needed because a single fidelity value can be misleading. A state may have high fidelity but no Wigner negativity. Conversely, a state may preserve some nonclassicality but have lower overall overlap.

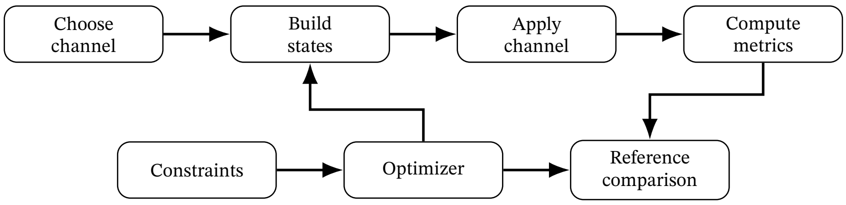

Figure 10. Workflow of the Quantum Teleportation State Explorer. The app configures a noisy teleportation channel, builds reference or optimized Fock-basis states, applies the channel, computes diagnostics, and compares the optimized state with reference states.

5.6. Optimized State Under a Saved or Imported Channel

The most direct app output is the fidelity comparison between the optimized imported state and the reference states under the same saved or imported channel. This is important because the optimized state should not be interpreted in isolation. It must be tested against familiar states under identical noise conditions.

As shown in Fig. 11, the optimized imported state has the highest fidelity for the selected channel. The coherent and squeezed vacuum states also perform well, while the more structured non-Gaussian states have lower fidelity. This is consistent with the physical picture that Gaussian blurring favors smoother phase-space distributions.

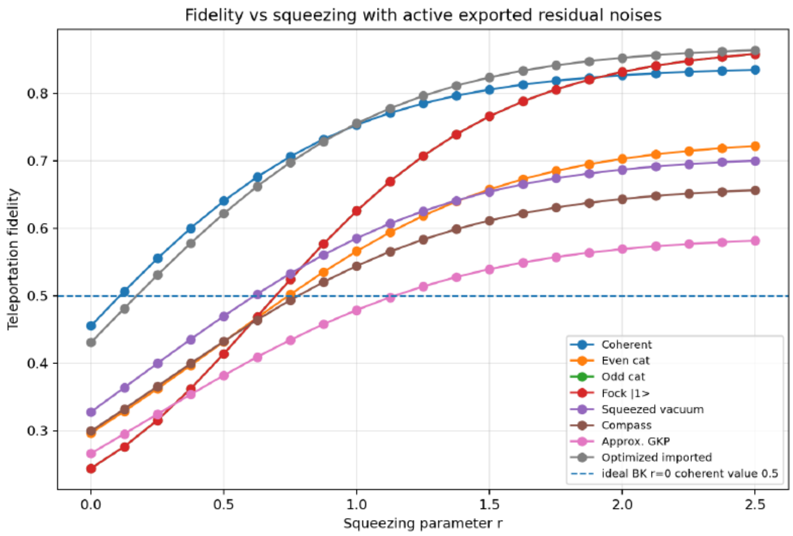

Figure 11. Teleportation fidelity under the saved or imported channel. The optimized imported state outperforms the standard reference states for this particular noise model and constraint set. This should be interpreted as channel adaptation rather than universal optimality.

5.7. Optimized Wigner Input and Output

The Wigner input-output comparison gives a more detailed view of what the optimizer found. Figure 12 shows that the optimized input state contains a central positive structure together with weak surrounding interference-like features. After teleportation, the output Wigner function is smoother because the noisy channel blurs fine phase-space structure.

This comparison is important because fidelity alone does not reveal the full structure of the optimized state. The input-output Wigner plot shows directly which features survive the channel and which features are washed out. In this case, the output remains localized and close to the input core, but the outer interference pattern is strongly reduced.

5.8. Fidelity Sweeps with Active Exported Residual Noises

The app also allows the optimized state and reference states to be tested under active exported residual noise settings. Figures 13 and 14 show fidelity versus squeezing for two exported noisy-channel configurations. In both cases, the optimized imported state performs competitively and can exceed the standard references over a significant squeezing range.

These plots demonstrate the main advantage of the app: after a state is optimized under one channel, it can be reinserted into parameter sweeps and compared with known states. The optimized state is therefore not just a single numerical vector; it becomes another test state that can be benchmarked across different channel qualities.

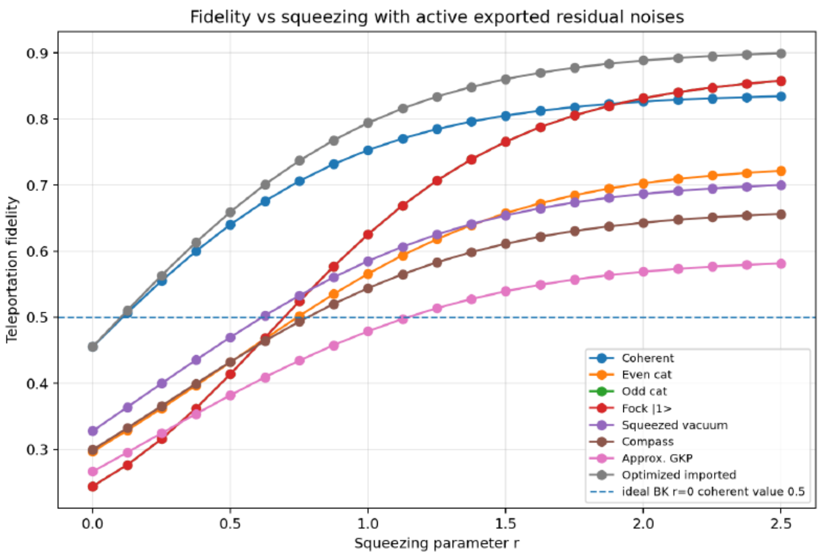

Figure 12. Wigner input-output comparison for the optimized imported state. The noisy channel preserves the central phase-space structure while suppressing weaker interference-like features.

The dashed line in the plots marks the ideal Braunstein–Kimble coherent-state classical benchmark $F = 0.5$. States above this line are performing above the standard coherent-state classical threshold, although this benchmark should not be interpreted as a universal classical limit for all non-Gaussian input states.

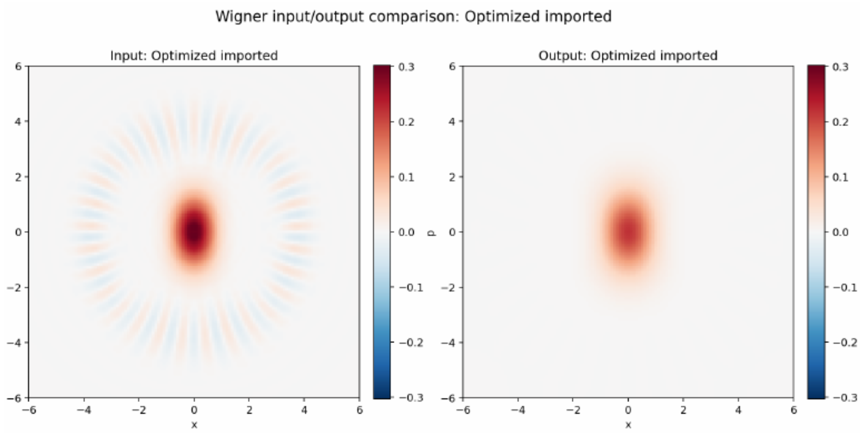

Figure 13. Fidelity versus squeezing with active exported residual noises. The optimized imported state remains highly competitive under the selected noisy-channel configuration.

5.9. Interpretation of the Optimized State

The optimized state should be interpreted as a channel-adapted state. It is not necessarily the best state for all teleportation scenarios. Its performance depends on the selected noise model, energy constraint, cutoff, objective function, and optional constraints. This is why the app compares the optimized state with coherent, squeezed, Fock, cat, compass, and approximate GKP-like states under identical channel settings.

Pure-fidelity optimization often favors states whose dominant Wigner structure is smooth and localized, because such states survive Gaussian blurring well. If the objective includes Wigner-negativity survival, the optimizer is encouraged to preserve nonclassical features. Thus, the answer to the question "which state is best?" depends on whether the goal is ordinary state overlap, survival of Wigner negativity, or another physical criterion.

6. NUMERICAL LIMITATIONS AND DISCUSSION

6.1. Finite Cutoff

The finite Fock cutoff is one of the most important numerical limitations. A small cutoff may be sufficient for smooth low-energy Gaussian states, but it may fail for displaced, highly non-Gaussian, or strongly noisy states. Approximate GKP-like states and compass states are especially demanding because they contain fine phase-space structure.

For optimized states, cutoff effects are even more important. The optimizer may exploit the boundary of the truncated Hilbert space if not constrained. Therefore, we monitor high-Fock tail population and compare selected results at $N_{\mathrm{cut}} = 10$ and $N_{\mathrm{cut}} = 30$.

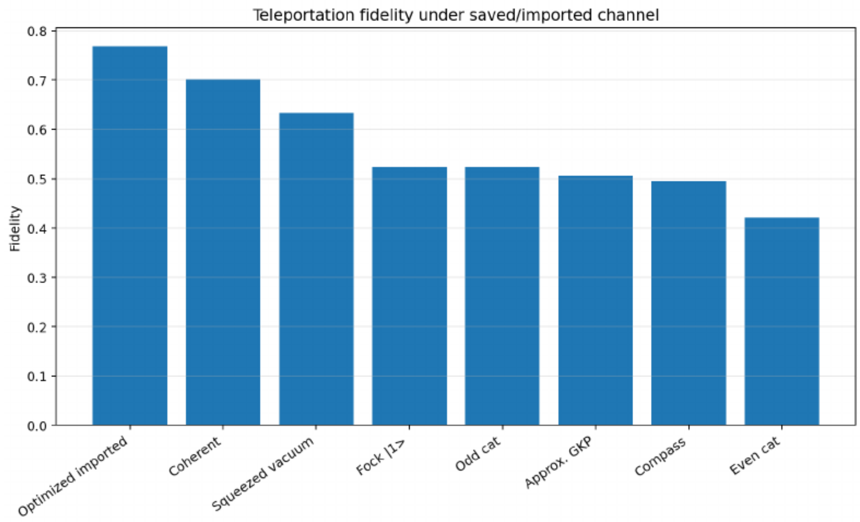

Figure 14. Second fidelity-versus-squeezing sweep with active exported residual noises. The optimized imported state is again competitive, showing that the app-generated state can be benchmarked against reference states across channel parameters.

6.2. Finite Wigner Grid

The Wigner-grid range and resolution also affect the results. If the grid is too small, broad output states are clipped. If the grid is too coarse, Wigner negativity and interference fringes are underestimated. This can affect both fidelity and negativity survival. Therefore, grid convergence is important for final quantitative claims, especially for cat, compass, and approximate GKP-like states.

6.3. Low-Efficiency Numerical Artifacts

The detector-efficiency model contains the term

$$\frac{1-\eta}{2\eta}, \tag{50}$$

which diverges as $\eta \to 0$. This makes very low detector efficiencies hard to simulate accurately. In this regime the channel adds very broad displacement noise, and a finite Fock basis may not be sufficient. Therefore, irregular behavior at very low η is treated as a numerical artifact unless verified by convergence tests.

6.4. Optimization Caveats

The optimization problem is nonlinear and finite-dimensional. Multiple starting points reduce the chance of finding only a poor local optimum, but they do not prove global optimality. Therefore, the optimized state should be interpreted as a numerically found channel-adapted state.

The result also depends on the objective function. Pure-fidelity optimization tends to favor smooth states. Joint fidelity and negativity-survival optimization favors states with nonclassical structure. Energy constraints, parity constraints, and tail constraints also affect the final state. Thus, the app is best understood as an exploratory tool for inverse design, not as a proof of a unique universal optimum.

6.5. Physical Interpretation

The main physical picture is that imperfect continuous-variable teleportation blurs the input state in phase space. Smooth Gaussian Wigner functions are robust. Fine interference structures and Wigner negativity are fragile. This explains why coherent states often have high fidelity, while cat, compass, Fock, and approximate GKP-like states require stronger squeezing or better detection to survive.

The optimized-state results add another layer to this picture. They show that one can search for states adapted to a chosen noise model. However, the optimal state depends on the channel, energy constraint, cutoff, and metric. Therefore, realistic teleportation should be analyzed as a state-dependent and metric-dependent process, not only by quoting one fidelity number.

6.6. Summary of Findings

The main findings are:

1. Increasing the squeezing parameter r improves fidelity because finite-squeezing noise decreases as e^{-2r}.
2. Increasing detector efficiency generally improves fidelity, although very low detector efficiencies are numerically difficult.
3. The geometry of EPR noise matters. Anisotropic, rotated, and correlated noise can change the ranking of input states.
4. Wigner-negativity survival provides information beyond ordinary fidelity.
5. The Quantum Teleportation State Explorer turns the problem into an inverse-design task by optimizing Fock-basis states under selected noisy channels and physical constraints.

Overall, the project shows that continuous-variable teleportation quality depends on the input state, the phase-space structure of the noise, the chosen diagnostic metric, and the numerical constraints used in the simulation.

REFERENCES

[1] E. P. Wigner, "On the quantum correction for thermodynamic equilibrium", *Physical Review*, vol. 40, no. 5, pp. 749–759, 1932. DOI: 10.1103/PhysRev.40.749

[2] M. Hillery, R. F. O'Connell, M. O. Scully, and E. P. Wigner, "Distribution functions in physics: Fundamentals", *Physics Reports*, vol. 106, no. 3, pp. 121–167, 1984. DOI: 10.1016/0370-1573(84)90160-1

[3] C. H. Bennett, G. Brassard, C. Crépeau, R. Jozsa, A. Peres, and W. K. Wootters, "Teleporting an unknown quantum state via dual classical and einstein-podolsky-rosen channels", *Physical Review Letters*, vol. 70, no. 13, pp. 1895–1899, 1993. DOI: 10.1103/PhysRevLett.70.1895

[4] C. C. Gerry and P. L. Knight, "Quantum superpositions and schrödinger cat states in quantum optics", *American Journal of Physics*, vol. 65, no. 10, pp. 964–974, 1997. DOI: 10.1119/1.18691

[5] S. L. Braunstein and H. J. Kimble, "Teleportation of continuous quantum variables", *Physical Review Letters*, vol. 80, no. 4, pp. 869–872, 1998. DOI: 10.1103/PhysRevLett.80.869

[6] A. Furusawa, J. L. Sørensen, S. L. Braunstein, C. A. Fuchs, H. J. Kimble, and E. S. Polzik, "Unconditional quantum teleportation", *Science*, vol. 282, no. 5389, pp. 706–709, 1998. DOI: 10.1126/science.282.5389.706

[7] D. Gottesman, A. Kitaev, and J. Preskill, "Encoding a qubit in an oscillator", *Physical Review A*, vol. 64, no. 1, p. 012 310, 2001. DOI: 10.1103/PhysRevA.64.012310 arXiv: quant-ph/0008040.

[8] W. P. Schleich, *Quantum Optics in Phase Space*. Berlin: Wiley-VCH, 2001, ISBN: 9783527294350.

[9] A. Kenfack and K. Życzkowski, "Negativity of the wigner function as an indicator of non-classicality", *Journal of Optics B: Quantum and Semiclassical Optics*, vol. 6, no. 10, pp. 396–404, 2004. DOI: 10.1088/1464-4266/6/10/003 arXiv: quant-ph/0406015.

[10] S. Glancy and H. M. d. Vasconcelos, "Methods for producing optical coherent state superpositions", *Journal of the Optical Society of America B*, vol. 25, no. 5, pp. 712–733, 2008. DOI: 10.1364/JOSAB.25.000712

[11] J. R. Johansson, P. D. Nation, and F. Nori, "QuTiP: An open-source python framework for the dynamics of open quantum systems", *Computer Physics Communications*, vol. 183, no. 8, pp. 1760–1772, 2012. DOI: 10.1016/j.cpc.2012.02.021 arXiv: 1110.0573 [quant-ph].

[12] J. R. Johansson, P. D. Nation, and F. Nori, "QuTiP 2: A python framework for the dynamics of open quantum systems", *Computer Physics Communications*, vol. 184, no. 4, pp. 1234–1240, 2013. DOI: 10.1016/j.cpc.2012.11.019 arXiv: 1211.6518 [quant-ph].